ComplexRep : Integrating Learned Representations to Enhance Complex-valued Data Transparency

Jongseok Kim, Woonggyu Min, Juyeop Kim and Ohyun Jo

***Abstract*—Complex-valued data, unlike real-valued data, requires consideration of intricate correlations and patterns. In particular, within learning frameworks based on real-valued computations, conventional input representations for complex numbers may fail to account for the correlations between the real and imaginary components, leading to potential inefficiencies. To address this issue, we propose a novel framework called ComplexRep, aimed at efficiently processing complex-valued data and enhancing its transparency. This framework transforms complex sequence data into a format similar to images, allowing for the consideration of inter-component correlations while improving overall model performance. The ComplexRep framework employs advanced techniques such as Information Addition and the proposed Learned Representation Integration (LRI) to strengthen low model complexity and high Initial Trial Success Probability (ITSP). Additionally, we enhance the reliability of our experiments by utilizing both public datasets and data collected from real-world environments. Extensive evaluation results demonstrate that our framework excels even under low signal-to-noise ratio (SNR) conditions, increasing the overall system efficiency. Notably, compared to previously used input formats, ComplexRep improves ITSP performance and reduces model complexity, thus proving its efficiency. Further experiments across various models confirm the framework's compatibility with several state-of-the-art models. All experiments include additional tests on real-world 5G data, validating the applicability of the proposed approach. This study presents the potential to effectively manage complex-valued data and maximize performance while offering directions for future complex-valued data processing research.**

***Index Terms*—Data Fusion, Complex-valued Data, Sequence Imagification, Information Addition, Sequence Reconstruction, Representation Stack, Representation Learning**

I. Introduction

DATA fusion is a crucial technique that combines various types of data to enhance the accuracy and transparency of information [1], [2]. Complex-valued data, in particular, exhibits diverse characteristics and requires consideration of intricate correlations and patterns during the fusion process [3], [4], [5]. Such data demands unique analytical approaches, providing valuable insights essential for developing high-performance analytical systems [6], [7]. Datasets composed of complex-valued data have distinct properties compared to real-valued data, and understanding and analyzing these datasets also contributes to improving the overall performance and stability of systems [8], [9], [10]. For instance, modulation is typically applied to ensure proper transmission of signals, while in the demodulation process, restoring modulated signals to their original form requires knowledge of the channel information, modulation scheme, and frequency used. Such information can be obtained by analyzing the Demodulation Reference Signal (DMRS) in commercial communication networks [11], [12]. Datasets used in modulation recognition and DMRS typically consist of complex-valued sequence signals. In real-world environments, it is essential to compare and analyze these signals to identify each sequence. Wang et al. [13] a sequence-based anomaly detection method was proposed to counter DMRS spoofing attacks in 5G NR systems. Gul et al. [14] addressed timing and frequency synchronization issues in Orthogonal Frequency Division Multiplexing (OFDM) systems using Zadoff–Chu sequences. Hua et al. [15] analyzed the effect of frequency offset on the timing performance of Zadoff–Chu sequences. Additionally, Wang et al. [16] enhanced automatic modulation classification performance using hybrid data augmentation and lightweight neural networks, and Pitaval et al. [17] proposed supersets of Zadoff–Chu sequences with low-correlation zones to overcome the 5G Physical Random Access Channel (PRACH) capacity shortfall. These studies highlight the importance of accurately comparing and analyzing complex-valued signals to identify each sequence in real-world communication environments. However, detecting and analyzing complex-valued signals can be challenging and time-consuming due to the need to consider the inter-component correlations [18], [19], [20], [21].

To address these challenges and improve the process, recent research has explored various techniques for complex-valued data. Zha et al. [22] developed a deep learning framework for signal modulation and multi-signal detection. Zhang et al. [23] proposed a deep learning approach for identifying coexisting signal types in shared spectrum environments. Chen et al. [24] introduced SigNet, a deep learning framework for signal classification with strong performance in small-sample learning. Mutlu and Kabalci [25] presented a deep learning-based method for improving channel estimation accuracy in 5G Multiple Input and Multiple Output (MIMO) systems. Wang et al. [26] addressed specific emitter identification using Complex-Valued Neural Networks (CVNN) combined with network compression to enhance performance and reduce model complexity. Notably, studies have focused on improving performance by training models with complex-valued

This paper expands upon the research published by the authors in the AAAI-24 conference proceedings.

Jongseok Kim, Woonggyu Min and Ohyun Jo are with the Department of Computer Science, Chungbuk National University, Chenogju 28644, South Korea (e-mail: kjseok@chungbuk.ac.kr, minwg1021@chungbuk.ac.kr, ohyunjo@chungbuk.ac.kr)

Juyeop Kim is with the Department of Electronics Engineering, Sookmyung Women's University, Yongsan-gu, South Korea (e-mail: jykim@sookmyung.ac.kr)

(*Corresponding Author: Ohyun Jo.*)

data [27], [28], [29]. While learning-based models exhibit strong performance in processing high-dimensional data such as complex-valued signals [30], [31], [32], they often face difficulties in adapting to practical system environments due to their complexity and high computational demands [33], [34], [35]. Moreover, recognizing and classifying complex-valued signals remain challenging tasks due to signal degradation caused by interference, distortion, and noise during the transmission process [36], [37], [38], [28].

To mitigate these issues, active research is being conducted on feature extraction during the learning process using complex-valued data and representation learning [39], [40]. Zheng et al. [41] proposed fusion methods to improve the performance of CNN-based automatic modulation classification when the signal length is variable. Dong et al. [42] introduced a deep Convolutional Neural Network (CNN)-based approach for channel estimation in mmWave massive MIMO systems, improving accuracy while reducing complexity. Zhang et al. [43] developed High-order Convolutional Attention Networks (HoCANs) to enhance automatic modulation classification performance, particularly in low SNR environments. Nie et al. [44] proposed a network that combines low-level and high-level features to improve the accuracy of complex-valued signal modulation type classification. Hermawan et al. [45] introduced a representation-based network that achieves high accuracy in complex-valued signal modulation type classification while using fewer filters. However, these studies use the same sample format without considering the correlation between elements within complex-valued data.

In this paper, we propose the ComplexRep framework, aimed at preserving the correlations of complex-valued signals and significantly enhancing the overall performance of models. While learning models typically entail high computational demands, our proposed framework transforms complex-valued data into a format similar to images, thereby greatly reducing model complexity. Additionally, we introduce the Learned Representation Integration (LRI) to learn the temporal representations of signals, utilizing them as training data to improve the performance of lightweight ComplexRep-based learning models. We validate the reliability and practicality of the proposed framework through experiments and analyses conducted on both public datasets and data collected from real 5G systems.

Accordingly, the contribution of this study is as follows:

- This study introduces the innovative **"ComplexRep"** framework for efficiently processing complex-valued data, significantly enhancing model prediction performance compared to existing complex-valued data processing methods.
- By applying ComplexRep, the number of model parameters is reduced by more than three times, demonstrating the efficiency and potential of ComplexRep.
- By introducing novel temporal representations through ComplexRep and Learned Representation Integration (LRI) — techniques developed by the authors for the first time — we enhance the model's performance, especially in low signal-to-noise ratio (SNR) environments.
- We validate the suitability of ComplexRep and LRI through state-of-the-art learning models, assessing the framework's generalization capability and potential.
- Experiments conducted with open datasets not only validate the practical applicability of the proposed approach, but the use of data collected from real-world 5G environments further enables the assessment of its potential in actual system scenarios.

This paper is structured as follows: Section 2 provides a review of the complex-valued data used in this study. Section 3 introduces the ComplexRep framework and its constituent modules. Section 4 presents the experimental results and provides a detailed analysis of the proposed method's performance. Finally, Section 5 concludes the paper with a summary and outlines potential directions for future research.

II. Preliminaries

This section describes the complex-valued signal model utilized in this study [46], [47]. Complex-valued data is fundamentally composed of In-phase (I) and Quadrature-phase (Q) components, which can be expressed as follows:

$$z[i] = z^I[i] + j \cdot z^Q[i] \tag{1}$$

$$z^{IQ} = \left\{ \begin{bmatrix} z^I[i] \\ z^Q[i] \end{bmatrix} \mid i = 0, 1, \ldots, N-1 \right\} \tag{2}$$

where z represents the complex-valued data, i denotes the i-th element of z, z^I signifies the In-phase component, z^Q denotes the Quadrature-phase component, and j is the imaginary unit satisfying $j^2 = -1$. Additionally, z^{IQ} follows the separated $z^I, z^Q \in R$ and can be represented as $z^{IQ} \in R^{2\times N}$, where N denotes the sequence length. IQ data, as complex-valued data, can be visualized on the complex plane, with the In-phase component represented on the horizontal axis and the Quadrature-phase component on the vertical axis. However, using this representation as input for learning models can require a large number of training parameters, which increases model complexity and demonstrates inefficiency in representation.

To address this issue, this study proposes the ComplexRep method, which enhances the efficiency and transparency of input data while preserving the original data values. Furthermore, it generates more robust data by incorporating various information obtainable from the complex plane, rather than relying solely on the original data. In particular, the amplitude and phase of each complex-valued data used in this paper can be expressed as follows:

$$A_i = |z[i]| = \sqrt{(z^I[i])^2 + (z^Q[i])^2} \tag{3}$$

$$\varphi_i = \arg(z[i]) = \tan^{-1}\left(\frac{z^Q[i]}{z^I[i]}\right) \tag{4}$$

where A_i signifies the distance from the origin to the complex-valued data, and φ_i denotes the phase formed by the complex-valued data with the positive real axis. Various information that can be derived, including these components, can be utilized through ComplexRep, which will be elaborated upon in Section 3.

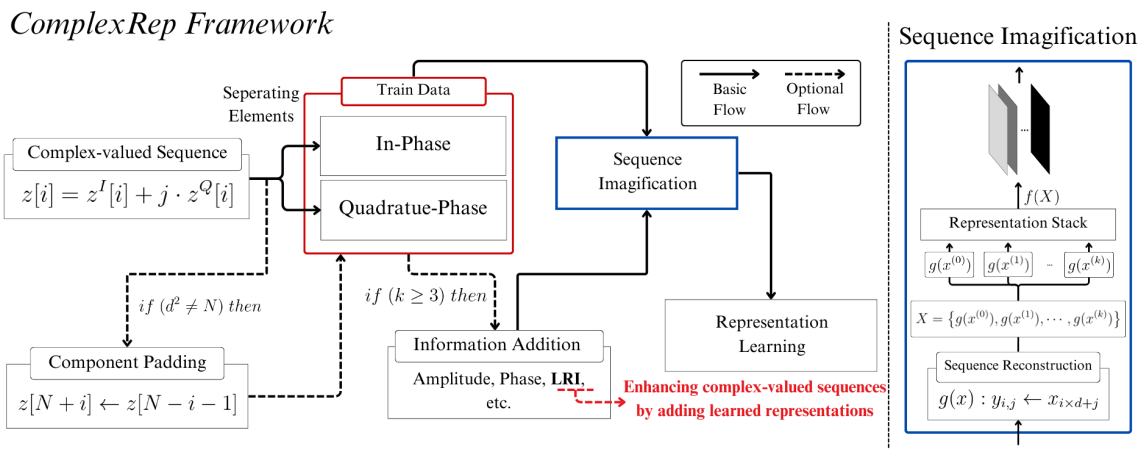

Fig. 1. Overall Structure of the ComplexRep Framework for Image-like Representation of Complex-Valued Data: Overall structure (left), Detailed structure of Sequence Imagification (right)

III. ComplexRep Framework

This section elaborates on the proposed ComplexRep process. Initially, the overall structure of the ComplexRep process is outlined. Subsequently, the additional proposed Learned Representation Integration(LRI) method is delineated.

A. ComplexRep Framework Process

The ComplexRep framework transforms signals into an image-like format to consider the correlations among the components of complex-valued data. Accordingly, ComplexRep includes various modules. Figure 1 illustrates the overall structure of the ComplexRep framework.

1) ***Component Padding****:* ComplexRep receives complex-valued data and analyzes it to determine whether the *Component Padding* is in progress. Component Padding serves as a preparatory step for Sequence Reconstruction, which is one of the stages of Sequence Imagification. Component Padding occurs when an element of a signal does not fulfill the required number of elements for the predetermined format. To enable efficient image processing, a square shape is adopted. The analysis process and the procedure for Component Padding can be expressed as follows:

$$z[N+i] \leftarrow z[N-i-1], \quad i \in [0, d^2 - N - 1] \tag{5}$$

where $z[N+i]$ indicates the position of the complex element added through Component Padding, and i denotes the range of the additional positions. Additionally, d represents the width of the side of the generated matrix and follows the relationship $d = \text{ceil}[\sqrt{N}]$. Furthermore, due to the application of the $ceil$ function, the input sequence length N may not be sufficient to completely fill the image, which is why Component Padding is initiated when $d^2 > N$. The additional components are appended in reverse sequential order, starting from the last element of the original sequence. Finally, the component added to the d^2-1 position serves as the last element of the generated sequence. The resulting complex-valued data is then passed to the next module with the I and Q components separated.

2) ***Information Addition****:* After the Component Padding process, the *Information Addition* module begins. This module determines the number of dimensions representing the depth of the image format, which is then conveyed to the next module, Sequence Imagification. In the Information Addition module, information extracted from the IQ data is combined with the original IQ data to enhance the richness of the resulting image and improve the transparency of the data. Commonly added information includes IQ coordinate-based data such as those in Eq.3 and Eq.4. Additionally, this study proposes LRI (Learned Representation Integration), which incorporates learned temporal information to enhance the robustness and transparency of the data, thereby improving performance. The details of LRI will be explained further in a subsequent section.

3) ***Sequence Reconstruction****:* The Sequence Imagification step consists of the *Sequence Reconstruction* and *Representation Stack* stages. Sequence Reconstruction refers to the process of converting the essential features into a predefined format for the image matrix. This process transforms a single sequence of data into an image matrix and can be expressed as follows:

$$g(x) : y_{i,j} \leftarrow x_{i \times d+j} \tag{6}$$

where x represents the input sequence data, and y denotes the output result of Sequence Reconstruction. The positions of each component are indicated by i and j, where $i, j \in [0, d-1]$. The input variable x can include both the original IQ data and the features output from the Information Addition module, which are then processed accordingly. The output matrix from the Sequence Reconstruction function $g(\cdot)$ can be expressed as follows:

$$y = \begin{bmatrix} x_0 & x_1 & \cdots & x_{d-1} \\ x_d & x_{d+1} & \cdots & x_{2d-1} \\ \vdots & \vdots & \ddots & \vdots \\ x_{(d-1)d} & x_{(d-1)d+1} & \cdots & x_{d^2-1} \end{bmatrix} \tag{7}$$

After the Sequence Reconstruction process, each feature takes the form of $R^{d \times d}$. This format allows for learning both spatial and temporal features, and when used with the

Algorithm 1 Componenet Padding and Sequence Reconstruction for Representation Stack

Input: One of Sequence Signal feature x → Eq.(2)
$N \leftarrow len(x)$
$d \leftarrow ceil[\sqrt{N}]$

Component Padding(x)**:**
  if $d^2 \neq N$ **then**
    Number of components to be created $d^2 - N$
    for $i = (0, \cdots, d^2 - N - 1)$ **do**
      $x[N + i] \leftarrow x[N - i - 1]$ → Eq.(5)
    end for
  end if

Sequence Reconstruction(x)**:**
i is Row, j is Column
  for $i = (0, \cdots, d - 1)$ **do**
    for $j = (0, \cdots, d - 1)$ **do**
      Matrix Traversal of $x_{i,j}$ with i and j → Eq.(7)
      Store $x_{i \times j + j}$ in $y_{i,j}$ matrix → Eq.(6), Eq.(7)
    end for
  end for

Output: $d \times d$ sequence feature matrix $y \in R^{d \times d}$

→ The input of Eq.(8)

Representation Stack module, it enhances the relationships between the components of the complex-valued data. Thus, compared to the original IQ data in the form of $R^{2 \times N}$, this method increases correlation between components. Algorithm 1 outlines the Sequence Reconstruction process within Imagification, with its output feeding into the Representation Stack module.

*4) **Representation Stack**:* After Sequence Reconstruction, the process moves on to the *Representation Stack* stage. Representation Stack plays a role similar to the RGB color model, creating a format where multiple pieces of information are included for each pixel. The RGB color model consists of three-dimensional data in the form of $R^{i \times j \times 3}$. In this paper, Representation Stack is performed based on the RGB model, which integrates various pieces of information for each pixel. The goal of Representation Stack is to combine features extracted from IQ data with the original IQ data, enriching the feature set while also enhancing the correlation between components. The input variables for Representation Stack can be expressed as follows:

$$X = \left\{ g(x^{(0)}), g(x^{(1)}), \cdots g(x^{(k-1)}) \right\} \tag{8}$$

where k is the number of features for Representation Stack, where $k \geq 2$. If only IQ data is utilized, $k = 2$, set as the default value for k. Representation Stack process with input variable X is denoted as:

$$f(X) : w_{i,j,k} \leftarrow g(x^{(k)})_{i \times d + j} \tag{9}$$

where w represents the output result of Representation Stack, which is the final result of the ComplexRep process. The variable k designates the allocated dimension and input data of X, with $k = 0$ and $k = 1$ in X representing IQ data. The complex-valued data processed through the Representation Stack stage is generated in a matrix format similar to a multi-dimensional image, which can be used immediately as input data.

In this study, we analyzed the Representation Stack up to $k = 4$ through experiments, adding a maximum of two types of information in the Information Addition module. A comparative experiment was conducted with feature combinations at $k = 4$ to investigate the impact of each feature on classification performance.

B. LRI : Learned Representation Integration

Typically, the most reliable features obtainable from complex-valued data are amplitude and phase. In fact, this study analyzes the addition of amplitude and phase features through the Information Addition module. While using amplitude and phase allows for simple and intuitive signal analysis, capturing the characteristics of some complex-valued sequence data or time-series data can be challenging. To address this issue, we propose a Learned Representation Integration (LRI) module. LRI enables the learning of patterns in complex-valued sequence data and captures the temporal dependencies between input data. To achieve this, LRI is designed to leverage models capable of extracting temporal representations. Specifically, it utilizes LSTM and Transformer models, which demonstrate exceptional performance with sequence data and are adept at recognizing and adapting to timing dependencies [48], [49], [50], [51], [52]. Additionally, LRI is used in conjunction with the proposed ComplexRep, enabling the learning of both spatial and temporal representations to leverage complementary features. This is achieved by combining the Imagification module of ComplexRep with the temporal representations extracted by LRI. In this case, the input for LRI's feature addition is in the form of $z^{IQ} \in R^{2 \times N}$, and when applying LSTM, the LRI cell function and its output can be expressed as follows:

$$h_t, c_t = r(z_t^{IQ}, h_{t-1}, c_{t-1}) \tag{10}$$

$$Output : h_{d^2} \in R^{1 \times d^2} \tag{11}$$

where z_t^{IQ} represents the t-th column vector of z^{IQ}. The variables h_t and c_t denote the hidden state and cell state of the LRI cell, respectively, and the function $r(\cdot)$ refers to the LRI cell function defined in [53]. Figure 2 illustrates the Sequence Imagification module using advanced feature additions based on LRI, as defined by Eq. 10 and Eq. 11. The red matrix represents the In-phase component, while the green matrix represents the Quadrature-phase component. Before applying complex-valued signal data to the Sequence Imagification module, the In-phase and Quadrature-phase components are used as inputs to the LRI. The sequence h_{d^2}, having passed through all the LRI gates, undergoes a Sequence Reconstruction process similar to other sequence features and is

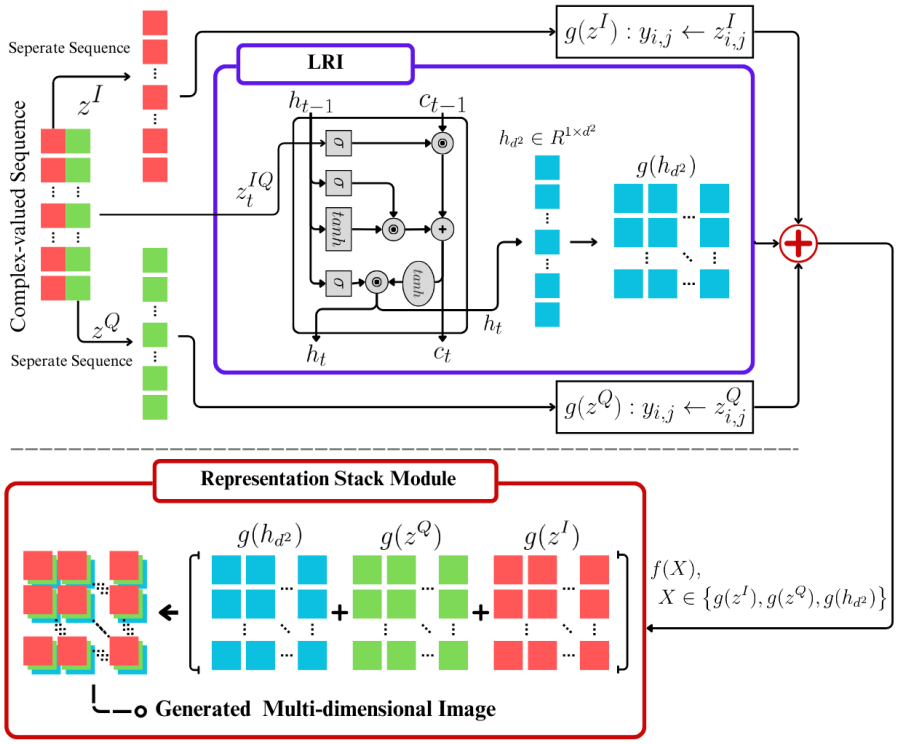

Fig. 2. Sequence Imagification Module with LRI for Complex-Valued Data Representation. (k = 3)

represented as a blue matrix, signifying the output of the LRI. When applying the Transformer [54], only the encoder portion is utilized, allowing for an output in the form $R^{1\times d^2}$, as shown in Eq. 11. Subsequently, all the representations that have passed through the Sequence Reconstruction process are used to generate a new multi-dimensional image through the Representation Stack. The generated image takes the form $R^{d\times d\times k}$, representing the RGB color structure. This multi-dimensional image serves as input to the learning model. In this study, we use LRI and ComplexRep together to extract diverse representations from complex-valued data and validate their performance.

IV. EXPERIMENT

A. Datasets

*1) **Overview of Public Datasets**:* We utilized public datasets from DeepSig: RadioML2016.10A and RadioML2018.01A public datasets for our performance evaluation[28], [55], [56]. Both datasets consist of 128 and 1024 complex elements, respectively, and contain samples collected in SNR environments ranging from -20 dB to 18 dB for RadioML2016.10A and from -20 dB to 30 dB for RadioML2018.01A. In addition, RadioML2016.10A provides 11 modulation types and 2018.01A provides 24 modulation types as labels. Due to the difference in modulation types between the two datasets, for consistent performance evaluation, we extracted 11 modulation types from RadioML2018.01A that are similar to the modulation types included in RadioML2016.10A and used the data with those labels. We also used data within the range of -12 dB to 6 dB for evaluation, as we considered that in environments with too high or too low SNR, there would be too much or too little noise in the signal to be comparable.

*2) **Dataset obtained in Real-World**:* To verify the applicability in real-world environments, we validate the performance of the proposed framework by utilizing DMRS data collected directly from real-world wireless communication environments as well as public datasets. For this purpose, the researchers built a system that simulates a real 5G network to capture signals in different SNR environments and collected data using two Universal Software Defined Radio (USRP) B210 devices [46]. The data collected is based on the signals generated during the wireless communication process between the gNodeB (gNB) and the user equipment (UE), and the researchers implemented each USRP device as a software modem to act as a gNB and UE. In addition, all functional blocks were designed in strict compliance with the latest 5G standards. The structure of implemented testbed and data collection process are shown in Figure 3.

The gNB generates a beam that covers a single cell area, while the UE performs initial cell selection and receives the Synchronization Signal Block (SSB). On the UE side, the USRP converts the RF signals received by the USRP into baseband signals and transmits them to the PC, which then performs cell search based on them. On the gNB side, the PC generates SSB baseband signals, which are then converted into RF signals by the USRP and transmitted to the wireless channel. In this study, all baseband functions, including 5G cell search, were implemented through self-developed software on the UE side, and were executed entirely software-based except for RF signal generation. In addition, during data acquisition and processing, two software threads, virtual RF

(vRF) and virtual search (vSRCH), cooperated to perform signal processing. vRF is responsible for RF signal processing, while vSRCH runs the cell search algorithm to derive search results. In particular, the blind detection function proposed in this work was performed within a vSRCH thread.

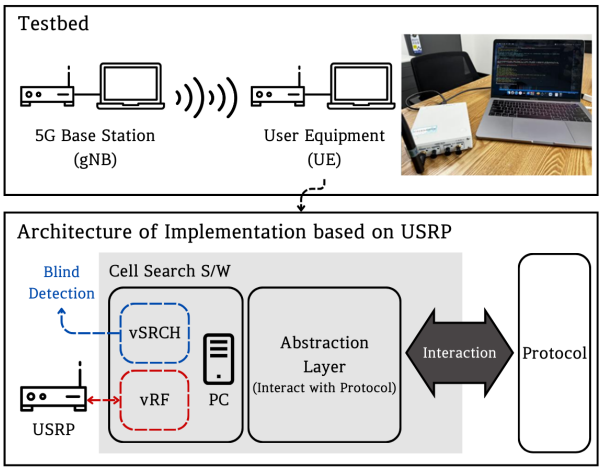

Fig. 3. Architecture of SDR-based 5G System for DMRS Data Collection

The Specifiaction of USRP, PC for collections and the details of collected 5G DMRS data is described in Table I. As shown in Table I, the experiments were conducted in 10 different SNR environments, and 8 DMRS indices were assigned from 0 to 7. For each index, 5000 samples were collected for a total of 40,000 samples, with one sequence consisting of 144 complex elements ($N = 144$). Also, Component Padding was not applied in this study, as it does not fulfill the condition $d^2 = N$.

TABLE I
SPECIFICATIONS OF USRP AND PC FOR DATA COLLECTION AND DMRS DATA DETAILS

Parameters	Value
CPU	Num of Cores : 6 Num of Threads : 12 Base Frequency : 3.70GHz
USRP(B210)	RF Coverage : 70MHz-6GHz Full Duplex, MIMO : 2-Tx, 2-Rx USB : 3.0 Connectivity
SNR	23.37 dB, 9.56 dB, -2.51 dB, -2.74 dB, -2.81 dB, -2.99 dB, -3.13 dB, -3.42 dB, -3.7 dB, -4.11 dB
Indices	index $\in [0, 7]$
Data by Index	5000
Number of Data by One SNR	8(indices) $\times$ 5000(data) = 40000
Component of Sequence	$z[i], i \in [0, 143]$
Number of One Sequence	N : 144
Component Padding or not	$(d^2 = N) \Rightarrow \neg ComponentPadding(\cdot)$
Image Dimension Range	$k \in \{2, 3, 4\}$

B. Evaluation Metrics

In this experiment, both *Initial Trial Success Probability (ITSP)* and *Average Trial(AT)* are used to evaluate the performance of the proposed method for modulation classification and demodulation index classification. These metrics play a crucial role in assessing the model's ability to effectively learn the patterns of modulation and demodulation signals and make accurate predictions.

Initial Trial Success Probability (ITSP) is a metric defined in the context of predicting and classifying signals within a real communication system. It represents the probability that the model correctly predicts the modulation scheme or demodulation index on the first attempt. This metric is expressed as follows:

$$\hat{y}_i = \underset{c}{\text{argmax}} P(c \mid s_i) \tag{12}$$

$$ITSP = \frac{1}{S} \sum_{i=0}^{S-1} I(\hat{y}_i = (y_i \mid s_i)) \tag{13}$$

where s_i represents the i-th signal, and all possible classes that can be assigned to the signal are denoted as c. S refers to the total number of signals. From this, the initial predicted value $\hat{y}_i$ for each signal s_i is derived. Subsequently, the number of instances where the actual class y_i matches the initially predicted $\hat{y}_i$ is obtained, defined using the indicator function $I(\cdot)$ [57]. ITSP evaluates the proportion of signals correctly predicted on the first attempt, reflecting the practical performance of a system handling modulation and demodulation signals.

Additionally, to comprehensively analyze ComplexRep in real-world environments, we employ the Average Trial. Average Trial represents the average number of attempts required for the model to accurately identify the modulation scheme or demodulation index of the signal. Unlike ITSP, Average Trial is a metric that evaluates the average number of attempts taken during the prediction process to correctly classify the signal. The Average Trial is expressed as follows:

$$\text{Average Trial}(AT) = \frac{1}{S} \sum_{i=0}^{S-1} (t \mid (r_i[t] = y_i) + 1) \tag{14}$$

where $r_i[t]$ represents the classes of probabilities sorted in descending order, t signifies the trial count minus one. For instance, when there are N classes denoted as $C_0, C_1, \cdots, C_{N-1}$, the classification model's probability value for each class are $p_0, p_1, \ldots, p_{N-1}$. The probabilities for the classes related to the i-th data are sorted in descending order by the classification model and denoted as r_i. The t-th element of r_i indicates the class with the $(t+1)$-th highest classification probability. Simultaneously, this implies that the $(t+1)$-th trial has been conducted to reach the actual class. In this case, t follows $t \in \{0, 1, \cdots, N-1\}$. Thus, Average Trial measures the number of attempts the model makes to produce an accurate prediction and represents the performance through its average. In this paper, we evaluate both accuracy and efficiency of the proposed process using ITSP and Average Trial. Additionally, we enhanced the credibility of the experiments by comparing the model parameters and FLOPs with

TABLE II
BASELINE PERFORMANCE COMPARISON OF SEQUENCE IMAGIFICATION USING COMPLEXREP AND CONVENTIONAL $R^{2\times d}$ FORMATS

Method	2016.10A				2018.01A				DMRS (Proprietary)			
	ITSP	AT	params	FLOPs	ITSP	AT	params	FLOPs	ITSP	AT	params	FLOPs
$R^{2\times d}$	0.586	2.135	4,517,003	31.45M	0.509	2.935	33,877,131,	247.90M	0.661	1.895	5,214,952	47.29M
Ours (k=2)	**0.609**	**2.056**	**1,483,595**	**13.93M**	**0.511**	**2.912**	**8,823,627**	**107.70M**	**0.721**	**1.796**	**1,676,152**	**21.59M**

TABLE III
IMPACT OF INFORMATION ADDITION ON DIMENSIONS AND PERFORMANCE METRICS IN COMPLEXREP

Dimensions(k)					2016.10A				2018.01A				DMRS (Proprietary)			
	A	φ	$I+Q$	$I-Q$	ITSP	AT	Params	FLOPs	ITSP	AT	Params	FLOPs	ITSP	AT	Params	FLOPs
$k=2$					**0.609**	**2.056**	1,483,595	13.93M	**0.511**	**2.912**	8,823,627	107.70M	**0.721**	**1.796**	1,676,152	21.59M
$k=3$	✓				**0.607**	2.095			0.491	2.971			**0.800**	1.565		
		✓			0.542	2.338	1,483,739	13.96M	**0.508**	2.954	8,823,771	107.99M	0.782	1.586	1,676,296	21.63M
			✓		0.606	**2.092**			0.495	**2.945**			0.797	**1.545**		
				✓	0.583	2.151			0.499	2.950			0.791	1.583		
$k=4$	✓	✓			0.526	2.405	1,483,883	14.00M	0.507	3.009	8,823,915	108.29M	0.799	1.550	1,676,440	21.67M
	✓		✓		0.575	2.126			**0.514**	2.936			0.801	1.543		
	✓			✓	**0.623**	2.061			0.510	2.955			**0.809**	**1.513**		
		✓	✓		0.525	2.389			0.511	2.955			0.798	1.554		
		✓		✓	0.616	2.082			0.505	2.955			0.796	1.548		
			✓	✓	0.611	**2.060**			0.512	**2.916**			0.798	1.545		

those of widely used models. For the classification model, we employed a lightweight version based on the VGGNet architecture, utilizing only the initial layers [58], [59].

C. Ablation Study

*1) **Baseline Analysis of ComplexRep**:* In the experiment, we conduct an ablation study not only to evaluate the overall performance of ComplexRep but also to assess the performance of its individual modules. To analyze the effectiveness of ComplexRep, we compare its performance with the conventional $R^{2\times d}$ format used in prior models. When evaluating the performance based on dimension k, ComplexRep without Information Addition is considered as $k = 2$. Additionally, for the case of 2016.10A, which consists of 128 components, Component Padding is required. However, to analyze the performance using only the intrinsic components of the signal, the experiment is conducted with a format of $R^{8\times 16\times 2}$. The Component Padding for 2016.10A is further validated in the Ablation Study. Considering these factors, Table II presents the baseline performance of Sequence Imagification using ComplexRep. Additionally, these results serve as the baseline performance across all experiments.

The experimental results demonstrate that ComplexRep outperforms the conventional $R^{2\times d}$ format across all datasets. Notably, in the DMRS data collected from real-world environments, ComplexRep improved ITSP by over 0.6 while reducing the model's parameters by more than threefold. This indicates that ComplexRep enhances classification accuracy while significantly reducing model complexity. The primary reason for this reduction in complexity is that ComplexRep streamlines the model's input shape. Additionally, Average Trial decreased as well, confirming the improved classification efficiency in real-world environments. Detailed ITSP and AT performance across different SNRs can be found in Appendix Table IX.

*2) **Impact of Information Addition on Dimension and Performance**:* Table III presents the changes in dimensions and corresponding performance results based on the Information Addition module. For the case where $k = 2$, no Information Addition is applied, and only the In-phase and Quadrature-phase are used, which represents the baseline ComplexRep. When one piece of information is added through Information Addition, it is defined as $k = 3$, and when two pieces are added, it is defined as $k = 4$. The additional information can be constructed using simple equations, such as Eq. (2) and Eq. (3). While there is a slight increase in Params and FLOPs as the dimension increases, this rise is negligible and does not significantly impact complexity. When comparing $k = 2$ and $k = 3$, a minor decrease in the performance of ITSP and AT can be observed for 2016.10A and 2018.01A. However, when $k = 4$ is used, adding the information A and $I - Q$ leads to performance improvement in 2016.10A, while adding A and $I + Q$ enhances the performance of 2018.01A. This demonstrates that the addition of appropriate information to each dataset can improve performance. In contrast, for the DMRS dataset, adding A at $k = 3$ results in an ITSP improvement of approximately 0.08 and a decrease in AT by 0.25, indicating performance enhancement. Additionally, with $k = 4$, where both A and $I-Q$ are added, the performance of both ITSP and AT further improves. The results on DMRS, collected in a real-world environment, validate the applicability of Information Addition and its effectiveness in real-world systems. Detailed performance at various SNR levels, according to dimension

TABLE IV
PERFORMANCE COMPARISON OF LEARNED REPRESENTATION INTEGRATION (LRI) ON RADIOML DATASETS

SNR	2016.10A						2018.01A					
	ITSP			AT			ITSP			AT		
	$R^{2\times d}$	LRI(LSTM)	LRI(Trans)	$R^{2\times d}$	LRI(LSTM)	LRI(Trans)	$R^{2\times d}$	LRI(LSTM)	LRI(Trans)	$R^{2\times d}$	LRI(LSTM)	LRI(Trans)
6 dB	**0.793**	0.781	0.688	**1.248**	1.263	1.526	**0.898**	0.896	0.887	1.142	**1.136**	1.146
4 dB	0.763	**0.793**	0.696	1.290	**1.244**	1.446	0.851	0.858	**0.852**	1.234	**1.193**	1.201
2 dB	0.785	**0.785**	0.694	1.275	**1.246**	1.434	**0.776**	0.751	0.753	1.414	1.382	**1.380**
0 dB	0.750	**0.775**	0.675	1.319	**1.254**	1.469	**0.646**	0.610	0.612	1.808	1.843	**1.802**
-2 dB	0.713	**0.761**	0.667	1.371	**1.282**	1.534	**0.512**	0.502	0.506	**2.509**	2.563	2.539
-4 dB	0.629	**0.709**	0.538	1.620	**1.446**	1.919	0.451	0.449	**0.452**	3.008	3.009	**2.987**
-6 dB	0.495	**0.562**	0.468	2.140	**1.982**	2.475	0.357	0.364	**0.369**	3.691	**3.649**	3.695
-8 dB	0.396	**0.435**	0.335	2.920	**2.815**	3.172	0.279	0.284	**0.285**	**4.255**	4.270	4.327
-10 dB	**0.296**	0.284	0.249	3.733	**3.686**	3.910	0.195	0.208	**0.218**	4.837	4.776	**4.759**
-12 dB	**0.242**	0.213	0.214	**4.431**	4.531	4.628	0.129	0.138	**0.148**	5.447	5.419	**5.362**
AVG	0.586	**0.610**	0.522	2.135	**2.075**	2.351	**0.509**	0.506	0.508	2.935	2.924	**2.920**

TABLE V
PERFORMANCE COMPARISON OF LEARNED REPRESENTATION INTEGRATION (LRI) ON DMRS DATASET

SNR	DMRS (Proprietary)					
	ITSP			AT		
	$R^{2\times d}$	LRI(LSTM)	LRI(Trans)	$R^{2\times d}$	LRI(LSTM)	LRI(Trans)
23.37 dB	1.000	1.000	1.000	1.000	1.000	1.000
9.56 dB	1.000	1.000	1.000	1.000	1.000	1.000
-2.51 dB	0.819	**0.941**	0.836	1.281	**1.100**	1.342
-2.74 dB	0.750	**0.930**	0.864	1.666	**1.138**	1.259
-2.81 dB	0.751	**0.937**	0.863	1.116	**1.110**	1.264
-2.99 dB	0.687	**0.907**	0.793	1.295	**1.182**	1.452
-3.13 dB	0.728	**0.881**	0.713	1.635	**1.235**	1.663
-3.42 dB	0.444	**0.834**	0.614	2.653	**1.339**	2.030
-3.7 dB	0.307	**0.417**	0.396	3.367	**2.731**	2.873
-4.11 dB	0.120	**0.230**	0.204	3.938	**3.738**	3.850
AVG	0.661	**0.808**	0.728	1.895	**1.557**	1.773

changes, can be found in Appendix Table X–XII.

*3) **Enhancing Performance with Learned Representation Integration**:* Increasing the dimension through Information Addition is an effective method to enhance performance, but determining which information to use and how to combine it can be challenging. To address this, we use Learned Representation Integration (LRI), which utilizes learned representations extracted from the original signal as additional information. The representation stacking process adopted the LRI obtained based on LSTM and Transformer as described in the previous section, both of which are capable of effectively capturing temporal representations. Table IV shows the performance of LRI on the RadioML dataset. For 2016.10A, except for three specific SNRs, the ComplexRep combined with LRI demonstrates superior ITSP performance. In particular, LRI using LSTM shows the best ITSP, and the Average Trial also improves significantly. On the other hand, for 2018.01A, LRI with Transformer enhances ITSP in all but four SNR cases. As for the Average Trial, applying LRI yields better performance across all but two SNRs. These results demonstrate that applying LRI offers superior performance compared to the standard approach and validates the efficiency of LRI. Table V provides the LRI performance on the DMRS dataset. In the DMRS dataset, except for the case of LRI (Trans) at -3.13dB, the framework with LRI outperforms the baseline ITSP across all other cases. Notably, LRI with LSTM demonstrates strong performance in both ITSP and Average Trial across all SNR levels. This indicates that by using the temporally learned representations obtained through LRI alongside ComplexRep, we achieved more robust data preprocessing. Furthermore, the performance improvements on the real-world collected dataset confirm the potential and practical applicability of the LRI module. To further analyze this, we also evaluated the complexity performance when applying LRI across different datasets. Table VI provides the performance results of LRI applied to each dataset. Applying ComplexRep and LRI (LSTM) to the 2016.10A dataset resulted in strong performance in both average ITSP and Average Trial, while significantly reducing model parameters and FLOPs. For the 2018.01A dataset, although the average ITSP saw a slight decrease, the model's complexity was reduced significantly, with parameters reduced by over threefold and FLOPs by more than twofold, showing much greater efficiency compared to existing methods. Additionally, applying ComplexRep and LRI to the real-world DMRS dataset demonstrated improved ITSP, Average Trial, model parameters, and FLOPs. The strong performance not only on open datasets but also on real-world data reinforces the practical viability of ComplexRep and LRI. Moreover, the reduced model complexity while maintaining high performance during training further validates the efficiency of the proposed framework.

*4) **Potential for State-Of-The-Art Model Application**:* To validate the practical potential of the ComplexRep framework and LRI, we applied them to models utilizing the Inception module, assessing their performance. These models were selected not only because they represent the latest advancements but also because Inception-based architectures can extract a broader range of features and representations. For the experiment, we applied LRI to VGG(Lightweight)[58], [59], InceptionV3[60], and InceptionResNetV2[61]. We also analyzed the results with the Sequence Imagification module ($k =$

TABLE VI
PERFORMANCE COMPARISON OF COMPLEXREP + LRI COMPARED TO CONVENTIONAL $R^{2\times d}$ FORMATS ACROSS DATASETS

Method	2016.10A				2018.01A				DMRS (Proprietary)			
	ITSP	AT	Params	FLOPs	ITSP	AT	Params	FLOPs	ITSP	AT	Params	FLOPs
$R^{2\times d}$	0.586	2.135	4,517,003	31.45M	**0.509**	2.935	33,877,131	247.90M	0.661	1.895	5,214,952	47.29M
Ours + LRI(LSTM)	**0.610**	**2.075**	1,550,811	**13.96M**	0.506	2.924	13,030,363	**107.99M**	**0.808**	**1.557**	1,842,760	**21.63M**
Ours + LRI(Trans)	0.522	2.351	**1,484,162**	14.37M	0.508	**2.920**	**8,824,194**	129.61M	0.728	1.773	**1,676,719**	22.13M

TABLE VII
PERFORMANCE COMPARISON OF STATE-OF-THE-ART MODELS AND LEARNED REPRESENTATION INTEGRATION (LRI)

Method	2016.10A				2018.01A				DMRS (Proprietary)			
	ITSP	AT	Params	FLOPs	ITSP	AT	Params	FLOPs	ITSP	AT	Params	FLOPs
VGG(Lightweight)[58], [59]	0.609	**2.056**	1,483,595	13.93M	**0.511**	**2.912**	8,823,627	107,70M	0.721	1.796	1,676,152	21.59M
VGG(Lightweight) + LRI(LSTM)	**0.610**	2.075	1,550,811	13.96M	0.506	2.924	13,030,363	107.99M	0.808	1.557	1,842,760	21.63M
VGG(Lightweight) + LRI(Trans)	0.522	2.351	1,484,162	14.37M	0.508	2.920	8,824,194	129.61M	**0.810**	**1.489**	1,676,719	21.13M
InceptionV3[60]	0.581	2.087	2,208,971	9.91M	0.524	**2.834**	17,282,251	138.66M	0.789	1.656	2,535,880	12.66M
InceptionV3 + LRI(LSTM)	**0.600**	2.098	2,276,331	9.93M	**0.526**	2.852	21,486,131	138.81M	**0.832**	1.579	2,620,840	12.68M
InceptionV3 + LRI(Trans)	0.592	**2.065**	2,209,682	10.34M	0.514	2.894	17,282,962	160.42M	0.817	**1.559**	2,536,591	13.19M
InceptionResNetV2[61]	0.572	2.195	545,355	3.05M	0.508	2.819	3,560,011	26.61M	0.828	**1.482**	610,120	3.51M
InceptionResNetV2 + LRI(LSTM)	**0.594**	**2.031**	612,715	3.07M	0.513	2.806	7,766,891	26.76M	0.812	1.486	695,080	3.53M
InceptionResNetV2 + LRI(Trans)	0.515	2.388	546,066	3.48M	**0.517**	**2.804**	3,560,722	48.37M	**0.829**	1.504	610,831	4.04M

TABLE VIII
PERFORMANCE ANALYSIS OF COMPLEXREP WITH COMPONENT PADDING ON THE 2016.10A DATASET

SNR	2016.10A							
	ITSP		AT		Params		FLOPs	
	$R^{2\times d}$	Component Padding	$R^{2\times d}$	Component Padding	$R^{2\times d}$	Component Padding	$R^{2\times d}$	Component Padding
6 dB	**0.793**	0.776	**1.248**	1.249	4,517,003	**1,614,667**	31.45M	**15.60M**
4 dB	0.763	**0.787**	1.290	**1.232**				
2 dB	0.785	**0.785**	1.275	**1.243**				
0 dB	**0.750**	0.748	1.319	**1.296**				
-2 dB	0.713	**0.738**	1.371	**1.339**				
-4 dB	0.629	**0.654**	1.620	**1.534**				
-6 dB	0.495	**0.556**	2.140	**1.905**				
-8 dB	0.396	**0.427**	2.920	**2.727**				
-10 dB	0.296	**0.305**	**3.733**	3.569				
-12 dB	**0.242**	0.222	**4.431**	4.615				
AVG	0.586	**0.600**	2.135	**2.071**	-	-	-	-

2) applied to these models. Table VII presents the performance comparison of these models with the integration of LRI. When applying VGG (Lightweight), there was a slight performance decline in both the 2016.10A and 2018.01A datasets. However, this can be mitigated by using more advanced models for training. Both InceptionV3 and InceptionResNetV2 showed improved ITSP when using LRI (LSTM) on 2016.10A, with enhancements also observed in Average Trial performance. While LRI (LSTM) performed well on both datasets, the increased model parameters due to LSTM, especially with longer sequences in 2018.10A, highlight a challenge to be addressed in future research. In the case of the DMRS dataset, all models achieved better performance when LRI was applied, with InceptionV3 combined with LRI (LSTM) recording the highest ITSP of 0.832. Moreover, LRI (Trans) applied to VGG (Lightweight) improved ITSP by approximately 0.089 and reduced Average Trial by about 0.317, demonstrating both accuracy and efficiency. Since the features and representations extracted by each model vary, selecting the appropriate LRI for each model can lead to further performance improvements. Appendix Table XIII–XVIII describe the performance of each model under different conditions in detail.

*5) **Effect of Component Padding**:* To ensure that ComplexRep can be applied to data with varying sequence lengths, a Component Padding module is introduced. To analyze its effectiveness, we require data where $d^2 \neq N$, and the 2016.10A dataset with a sequence length of 128 is suitable for this purpose. Table VIII presents the results of ComplexRep with component padding applied to the 2016.10A dataset. Introducing the Component Padding module increases the sequence length of the data, but it does not lead to an increase in model parameters or FLOPs. In fact, the model parameters and FLOPs are reduced by more than half, due to the complexity reduction achieved through the Sequence Imagification module following Component Padding. Additionally, both ITSP and Average Trial improved across most SNR levels, with only a few exceptions. When comparing average performance, applying the ComplexRep framework with Component Padding resulted in better performance than the baseline. This demonstrates that, despite increasing sequence length, ComplexRep effectively reduces complexity while improving performance. Moreover, it confirms that ComplexRep is not only suitable for data with varying sequence lengths but also practical for real-world applications.

TABLE IX
DETAILED ITSP AND AVERAGE TRIAL RESULTS ACROSS SNR LEVELS FOR BASELINE COMPLEXREP

SNR	2016.10A				2018.01A			
	ITSP		AT		ITSP		AT	
	$R^{2\times d}$	Ours (k=2)	$R^{2\times d}$	Ours (k=2)	$R^{2\times d}$	Ours (k=2)	$R^{2\times d}$	Ours (k=2)
6 dB	0.793	**0.799**	1.248	**1.238**	**0.898**	0.879	**1.142**	1.178
4 dB	0.763	**0.799**	1.290	**1.232**	**0.851**	0.844	**1.234**	1.239
2 dB	0.785	**0.812**	1.275	**1.218**	0.776	**0.779**	1.414	**1.384**
0 dB	0.750	**0.770**	1.319	**1.280**	0.646	**0.652**	1.808	**1.789**
-2 dB	0.713	**0.750**	1.371	**1.330**	**0.512**	0.509	**2.509**	2.547
-4 dB	0.629	**0.677**	1.620	**1.538**	0.451	**0.459**	3.008	**2.991**
-6 dB	0.495	**0.558**	2.140	**1.958**	0.357	**0.369**	3.691	**3.560**
-8 dB	0.396	**0.426**	2.920	**2.678**	0.279	**0.283**	4.255	**4.186**
-10 dB	0.296	**0.296**	3.733	**3.636**	0.195	**0.201**	4.837	**4.777**
-12 dB	**0.242**	0.206	**4.431**	4.453	0.129	**0.133**	**5.447**	5.472
AVG	0.586	**0.609**	2.135	**2.056**	0.509	**0.511**	2.935	**2.912**

SNR	DMRS (Proprietary)			
	ITSP		AT	
	$R^{2\times d}$	Ours (k=2)	$R^{2\times d}$	Ours (k=2)
23.37 dB	1.000	1.000	1.000	1.000
9.56 dB	1.000	1.000	1.000	1.000
-2.51 dB	0.819	**0.828**	1.281	**1.348**
-2.74 dB	0.750	**0.842**	1.666	**1.322**
-2.81 dB	0.751	**0.859**	**1.116**	1.284
-2.99 dB	0.687	**0.786**	**1.295**	1.471
-3.13 dB	**0.728**	0.726	1.635	**1.635**
-3.42 dB	0.444	**0.599**	2.653	**2.076**
-3.7 dB	0.307	**0.357**	3.367	**3.005**
-4.11 dB	0.120	**0.212**	3.938	**3.818**
AVG	0.661	**0.721**	1.895	**1.796**

V. CONCLUSION

This study demonstrated the effectiveness and practicality of the ComplexRep framework and Learned Representation Integration (LRI) for complex-valued data. To ensure reliability, we conducted experiments not only on open datasets but also on a real-world dataset that we collected ourselves. ComplexRep showed outstanding performance on both open datasets and the real-world DMRS dataset. Various modules within ComplexRep contributed to reducing computational complexity while improving ITSP and Average Trial performance. The application of LRI, which strengthens temporal representations, proved both efficient and performance-enhancing, consistently delivering high results even on state-of-the-art models. Future work will focus on developing more efficient methods for applying LRI to long sequence data and validating ComplexRep's applicability across a wider range of real-world datasets.

VI. ACKNOWLEDGMENT

This work was supported by the Institute of Information & communications Technology Planning & Evaluation(IITP) grant funded by the Korea government(MSIT) (No. 2021-0-00165, Development of 5G+ Intelligent Basestation Software Modem). In part, this work was also supported by the National Research Foundation of Korea(NRF) grant funded by the Korea government(MSIT). (No. 2021R1A2C2095289).

VII. APPENDIX

A. Detailed Results for Baseline ComplexRep

Table IX presents the results of experiments conducted across various SNRs, as discussed in Section IV-C1. When applying the proposed framework to the 2016.10A dataset, performance improvements were observed for both ITSP and Average Trial at all SNR levels, except for -12 dB. For 2018.01A, while some high-SNR cases saw decreases in ITSP and Average Trial performance, the Sequence Imagification module contributed to improvements as the SNR decreased. In experiments conducted on the DMRS dataset collected in a real environment, ITSP performance improved at most SNRs, with notable gains of over 0.1 at -2.74 dB and -3.42 dB, underscoring the prediction capability of the proposed framework. For Average Trial, performance consistently decreased by more than 0.1 on average compared to traditional methods, further validating the practicality and efficiency of the framework in real-world scenarios.

TABLE X
PERFORMANCE OF INFORMATION ADDITION FOR THE 2016.10A DATASET

2016.10A											
SNR	Dimensions(k)	k=3				k=4					
	A	✓				✓	✓	✓			
	φ		✓			✓			✓	✓	
	$I+Q$			✓			✓		✓		✓
	$I-Q$				✓			✓		✓	✓
6 dB	ITSP	**0.802**	0.716	0.785	0.755	0.696	0.775	**0.801**	0.696	0.794	0.793
	AT	**1.225**	1.476	1.261	1.297	1.516	1.282	1.227	1.541	**1.217**	1.262
4 dB	ITSP	**0.815**	0.730	0.795	0.796	0.689	0.754	**0.817**	0.689	0.817	0.775
	AT	**1.210**	1.378	1.225	1.239	1.499	1.294	**1.203**	1.454	1.205	1.248
2 dB	ITSP	**0.818**	0.730	0.795	0.785	0.684	0.748	0.809	0.695	**0.828**	0.779
	AT	**1.211**	1.352	1.240	1.254	1.432	1.309	1.209	1.423	**1.190**	1.244
0 dB	ITSP	**0.796**	0.708	0.773	0.759	0.678	0.701	**0.828**	0.670	0.808	0.797
	AT	**1.242**	1.371	1.271	1.289	1.428	1.382	**1.200**	1.438	1.220	1.218
-2 dB	ITSP	0.748	0.695	**0.750**	0.713	0.666	0.710	**0.782**	0.664	0.781	0.755
	AT	1.336	1.412	**1.315**	1.372	1.460	1.399	**1.283**	1.484	1.283	1.305
-4 dB	ITSP	0.665	0.598	**0.695**	0.659	0.612	0.632	0.695	0.579	0.698	**0.715**
	AT	1.552	1.726	**1.480**	1.564	1.728	1.618	1.490	1.852	1.483	**1.446**
-6 dB	ITSP	0.539	0.465	**0.564**	0.537	0.447	0.521	0.545	0.457	**0.551**	0.546
	AT	2.034	2.395	**2.008**	2.089	2.514	2.090	1.995	2.394	**2.007**	2.022
-8 dB	ITSP	**0.393**	0.345	0.388	0.353	0.363	0.387	0.419	0.361	0.426	**0.431**
	AT	**2.865**	3.276	2.915	3.099	3.322	2.841	2.741	3.304	2.825	**2.689**
-10 dB	ITSP	0.277	0.250	**0.299**	0.277	0.243	0.284	**0.319**	0.274	0.266	0.310
	AT	3.786	4.093	**3.641**	3.816	4.185	3.625	3.666	4.014	3.875	**3.606**
-12 dB	ITSP	0.211	0.180	**0.219**	0.197	0.185	**0.235**	0.211	0.165	0.189	0.212
	AT	**4.486**	4.902	4.560	4.493	4.963	**4.425**	4.597	4.993	4.511	4.555
AVG	ITSP	**0.607**	0.542	0.606	0.583	0.526	0.575	**0.623**	0.525	0.616	0.611
	AT	2.095	2.338	**2.092**	2.151	2.405	2.126	2.061	2.389	2.082	**2.060**

TABLE XI
PERFORMANCE OF INFORMATION ADDITION FOR THE 2018.01A DATASET

2018.01A											
	Dimensions(k)	k=3				k=4					
	A	✓				✓	✓	✓			
SNR	φ		✓			✓			✓	✓	
	$I+Q$			✓			✓		✓		✓
	$I-Q$				✓			✓		✓	✓
6 dB	ITSP	0.861	0.875	0.872	**0.882**	0.885	0.888	0.872	0.890	0.876	**0.890**
	AT	1.193	1.207	1.190	**1.178**	1.184	1.176	1.219	1.175	1.198	**1.158**
4 dB	ITSP	0.815	**0.850**	0.826	0.833	0.860	0.864	0.853	0.865	0.853	**0.871**
	AT	1.273	**1.247**	1.258	1.251	1.242	1.228	1.271	1.227	1.245	**1.191**
2 dB	ITSP	0.719	**0.777**	0.724	0.726	0.790	**0.799**	0.785	0.796	0.784	0.796
	AT	1.471	**1.418**	1.470	1.471	1.400	1.383	1.407	1.372	1.399	**1.351**
0 dB	ITSP	0.590	**0.628**	0.588	0.592	0.628	0.644	**0.645**	0.631	0.618	0.633
	AT	2.007	**1.887**	1.957	1.968	1.960	1.890	**1.835**	1.873	1.903	1.849
-2 dB	ITSP	0.491	0.493	**0.494**	0.493	0.498	**0.495**	0.498	0.496	0.493	0.495
	AT	2.752	2.647	2.657	**2.637**	2.755	2.676	2.680	**2.625**	2.631	2.653
-4 dB	ITSP	0.450	0.448	**0.453**	0.449	0.444	0.449	**0.453**	0.439	0.443	0.446
	AT	3.068	**3.067**	3.080	3.081	3.228	3.076	3.109	3.114	**3.059**	3.068
-6 dB	ITSP	0.359	0.360	0.363	**0.370**	0.356	0.366	**0.366**	0.361	0.356	0.361
	AT	**3.627**	3.703	3.715	3.673	3.776	3.698	3.676	3.719	3.689	**3.592**
-8 dB	ITSP	0.282	**0.285**	0.279	0.283	0.276	**0.291**	0.282	0.283	0.276	0.286
	AT	**4.163**	4.299	4.201	4.204	4.283	4.182	4.212	4.254	4.284	**4.180**
-10 dB	ITSP	0.210	0.222	0.216	**0.224**	0.205	0.212	0.211	0.206	0.212	**0.205**
	AT	4.723	4.688	**4.596**	4.687	4.822	**4.703**	4.747	4.791	4.772	4.731
-12 dB	ITSP	0.135	**0.143**	0.134	0.139	0.131	0.137	0.135	**0.143**	0.141	0.135
	AT	5.429	5.379	**5.329**	5.347	5.441	**5.344**	5.395	5.401	5.373	5.384
AVG	ITSP	0.491	**0.508**	0.495	0.499	0.507	**0.514**	0.510	0.511	0.505	0.512
	AT	2.971	2.954	**2.945**	2.950	3.009	2.936	2.955	2.955	2.955	**2.916**

TABLE XII
PERFORMANCE OF INFORMATION ADDITION USING DMRS DATA COLLECTED IN A REAL ENVIRONMENT

DMRS (Proprietary)											
	Dimensions(k)	k=3				k=4					
	A	✓				✓	✓	✓			
SNR	φ		✓			✓			✓	✓	
	$I+Q$			✓			✓		✓		✓
	$I-Q$				✓			✓		✓	✓
23.37 dB	ITSP	1.000	1.000	1.000	1.000	1.000	1.000	1.000	1.000	1.000	1.000
	AT	1.000	1.000	1.000	1.000	1.000	1.000	1.000	1.000	1.000	1.000
9.56 dB	ITSP	1.000	1.000	1.000	1.000	1.000	1.000	1.000	1.000	1.000	1.000
	AT	1.000	1.000	1.000	1.000	1.000	1.000	1.000	1.000	1.000	1.000
-2.51 dB	ITSP	**0.915**	0.901	0.899	0.901	**0.925**	0.916	0.924	0.912	0.900	0.918
	AT	**1.156**	1.181	1.196	1.191	**1.135**	1.146	1.141	1.160	1.193	1.150
-2.74 dB	ITSP	**0.933**	0.907	0.902	0.894	0.880	0.888	0.893	**0.910**	0.879	0.909
	AT	**1.125**	1.168	1.186	1.207	1.244	1.220	1.209	**1.164**	1.227	1.174
-2.81 dB	ITSP	**0.920**	0.910	0.911	0.910	**0.919**	0.916	0.907	0.915	0.905	0.919
	AT	**1.147**	1.164	1.167	1.169	**1.144**	1.152	1.170	1.159	1.183	1.150
-2.99 dB	ITSP	0.873	0.872	**0.876**	0.874	0.883	**0.896**	0.892	0.867	0.877	0.877
	AT	1.249	1.255	**1.246**	1.256	1.228	**1.193**	1.208	1.271	1.245	1.236
-3.13 dB	ITSP	**0.832**	0.815	0.811	0.802	**0.858**	0.836	0.853	0.814	0.827	0.806
	AT	**1.363**	1.380	1.404	1.428	**1.287**	1.330	1.292	1.383	1.345	1.393
-3.42 dB	ITSP	**0.795**	0.618	0.755	0.739	0.772	**0.778**	0.775	0.754	0.707	0.739
	AT	**1.450**	1.977	1.566	1.614	1.520	**1.495**	1.507	1.574	1.704	1.603
-3.7 dB	ITSP	0.500	0.531	0.506	**0.545**	0.474	0.508	0.562	0.562	**0.600**	0.565
	AT	2.407	2.288	2.407	**2.247**	2.496	2.377	2.167	2.191	**2.039**	2.161
-4.11 dB	ITSP	0.229	0.265	**0.310**	0.239	0.277	0.272	**0.280**	0.244	0.262	0.244
	AT	3.750	3.444	**3.274**	3.717	3.448	3.524	**3.437**	3.640	3.541	3.586
AVG	ITSP	**0.800**	0.782	0.797	0.791	0.799	0.801	**0.809**	0.798	0.796	0.798
	AT	1.565	1.586	**1.545**	1.583	1.550	1.543	**1.513**	1.554	1.548	1.545

B. Performance Analysis of Information Addition Across Varying SNR Levels

Information Addition is essential for observing how performance varies across different SNRs depending on the combined information. To this end, Table X–XII presents the performance of Information Addition across various SNRs not included in Table III of Section IV-C2. First, Table X presents the performance of information addition for the 2016.10A dataset. In terms of ITSP, the performance of the $k = 4$ configuration, which adds two pieces of information, is superior to that of the $k = 3$ configuration. Notably, at 0dB, adding $I-Q$ to A improves ITSP by 0.032. This demonstrates that the choice of additional information in the Information Addition module significantly impacts performance, validating that appropriate information combinations can lead to performance enhancements.

Table XI presents the performance of Information Addition for the 2018.01A dataset. Generally, the $k = 4$ configuration demonstrates superior performance compared to the $k = 3$ configuration across most SNR levels, validating the positive effects of additional information. Notably, at 0 dB, the addition of $I-Q$ to configuration A results in an increase of over 0.05 in ITSP performance, indicating a clear enhancement. This trend persists across other SNR levels, where the performance of the $k = 4$ configuration often surpasses that of $k = 3$ in both ITSP and Average Trial metrics. For instance, at 4 dB, the $k = 4$ configuration achieves a maximum AT performance of 1.191, showing a significant improvement compared to the results of $k = 3$, emphasizing the effectiveness of Information Addition in enhancing the system's noise resilience. Even at a low SNR of -8 dB, the ITSP performance of the $k = 4$ configuration remains stable at 0.291, while the AT value also records a low score, indicating that the added information contributes to maintaining robust performance. These results underscore that performance can be improved through appropriate combinations of information across various SNR levels. Significant enhancements are particularly observed at high and medium SNR levels, demonstrating that strategically selected information combinations increase the efficiency of both ITSP and Average Trial, thereby supporting the system's robustness and adaptability in noisy environments.

Table XII illustrates the performance of information addition using DMRS data collected in a real environment. The experimental results show that in high SNR ranges (23.37 dB and 9.56 dB), the information addition technique achieves a high success rate, with both ITSP and Average Trial values approaching 1.000. This indicates that information addition is effectively performed in stable communication environments. In the medium SNR range (-2.51 dB and -2.74 dB), relatively high performance was maintained, particularly with ITSP values exceeding 0.9 for most combinations. This suggests that the information addition technique remains effective at certain SNR levels. Notably, at -3.42 dB, when only A was added, the ITSP and Average Trial values recorded were 0.795 and 1.450, respectively, indicating that, in some SNR scenarios, not adding additional information may be more efficient. Through this analysis, this study empirically demonstrates that information addition techniques can effectively operate across

TABLE XIII
LRI PERFORMANCE ON **VGG (LIGHTWEIGHT)** ACROSS **RADIOML** DATASETS AT VARIOUS SNRS

VGG(Lightweight)[58], [59]												
SNR	2016.10A						2018.01A					
	ITSP			AT			ITSP			AT		
	k=2 (I, Q)	LRI(LSTM)	LRI(Trans)	k=2 (I, Q)	LRI(LSTM)	LRI(Trans)	k=2 (I, Q)	LRI(LSTM)	LRI(Trans)	k=2 (I, Q)	LRI(LSTM)	LRI(Trans)
6 dB	**0.799**	0.781	0.688	**1.238**	1.263	1.526	0.879	**0.896**	0.887	1.178	**1.136**	1.146
4 dB	**0.799**	0.793	0.696	**1.232**	1.244	1.446	0.844	**0.858**	0.852	1.239	**1.193**	1.201
2 dB	**0.812**	0.785	0.694	**1.218**	1.246	1.434	**0.779**	0.751	0.753	1.384	1.382	**1.380**
0 dB	0.770	**0.775**	0.675	1.280	**1.254**	1.469	**0.652**	0.610	0.612	**1.789**	1.843	1.802
-2 dB	0.750	**0.761**	0.667	1.330	**1.282**	1.534	**0.509**	0.502	0.506	2.547	2.563	**2.539**
-4 dB	0.677	**0.709**	0.538	1.538	**1.446**	1.919	**0.459**	0.449	0.452	2.991	3.009	**2.987**
-6 dB	0.558	**0.562**	0.468	**1.958**	1.982	2.475	0.369	0.364	**0.369**	**3.560**	3.649	3.695
-8 dB	0.426	**0.435**	0.335	**2.678**	2.815	3.172	0.283	0.284	**0.285**	**4.186**	4.270	4.327
-10 dB	**0.296**	0.284	0.249	**3.636**	3.686	3.910	0.201	0.208	**0.218**	4.777	4.776	**4.759**
-12 dB	0.206	0.213	**0.214**	**4.453**	4.531	4.628	0.133	0.138	**0.148**	5.472	5.419	**5.362**
AVG	0.609	**0.610**	0.522	**2.056**	2.075	2.351	**0.511**	0.506	0.508	**2.912**	2.924	2.920

TABLE XIV
LRI PERFORMANCE ON **INCEPTIONV3** ACROSS **RADIOML** DATASETS AT VARIOUS SNRS

InceptionV3 [60]												
SNR	2016.10A						2018.01A					
	ITSP			AT			ITSP			AT		
	k=2 (I, Q)	LRI(LSTM)	LRI(Trans)	k=2 (I, Q)	LRI(LSTM)	LRI(Trans)	k=2 (I, Q)	LRI(LSTM)	LRI(Trans)	k=2 (I, Q)	LRI(LSTM)	LRI(Trans)
6 dB	0.763	0.775	**0.783**	1.296	**1.269**	1.272	0.911	**0.915**	0.889	1.114	**1.113**	1.158
4 dB	0.731	0.763	**0.773**	1.327	**1.281**	1.282	0.871	**0.878**	0.853	1.177	**1.173**	1.209
2 dB	0.728	0.757	**0.772**	1.319	**1.276**	1.281	0.783	**0.799**	0.757	1.335	**1.327**	1.381
0 dB	0.720	0.738	**0.739**	1.343	**1.305**	1.315	0.626	**0.633**	0.620	1.796	**1.793**	1.833
-2 dB	**0.729**	0.725	0.717	1.338	**1.329**	1.369	0.503	**0.514**	0.508	2.551	**2.443**	2.580
-4 dB	0.668	**0.685**	0.666	1.529	**1.473**	1.525	**0.461**	0.453	0.459	3.002	**2.957**	3.025
-6 dB	**0.555**	0.541	0.537	2.015	**1.965**	2.061	0.387	**0.391**	0.387	**3.497**	3.530	3.559
-8 dB	0.415	**0.428**	0.403	2.749	**2.665**	2.765	**0.296**	0.295	0.295	**4.115**	4.212	4.157
-10 dB	0.283	**0.305**	0.303	3.546	3.526	**3.479**	**0.238**	0.234	0.226	**4.516**	4.647	4.655
-12 dB	0.220	0.221	**0.225**	4.403	**4.217**	4.297	**0.164**	0.149	0.143	**5.239**	5.330	5.380
AVG	0.581	**0.594**	0.592	2.087	**2.031**	2.065	0.524	**0.526**	0.514	**2.834**	2.852	2.894

various SNR environments, providing foundational data that can contribute to the design and improvement of real systems through a data-driven approach. By systematically analyzing performance changes according to SNR, the study presents optimization directions for information addition techniques, which can serve as a basis for future research.

C. Evaluation of ComplexRep and LRI in State-of-the-Art Models Under Various SNR Conditions

Table XIII presents the performance evaluation results of the proposed LRI (Learned Representation Integration) technique for the VGG (Lightweight) model, tested on the RadioML datasets 2016.10A and 2018.01A across various SNR levels. In both ITSP and Average Trial metrics, the performance of LRI configurations, such as LRI (LSTM) and LRI (Trans), is compared against the baseline combination of k=2 (I, Q) components. For 2016.10A, LRI (LSTM) demonstrates robust performance in terms of ITSP. However, for 2018.01A, a tendency toward performance degradation is observed at certain SNR levels. This indicates that the VGG (Lightweight) architecture in RadioML is too simple to learn deep representations and features effectively. It highlights the importance of model suitability for the dataset, suggesting that performance can be maximized when utilizing the appropriate model alongside ComplexRep and LRI. To demonstrate this, we conducted experiments using VGG (Lightweight) with LRI applied to the DMRS dataset. Table XV shows the results of evaluating DMRS data under various SNR conditions using the VGG (Lightweight) model with LRI applied. Except for -3.7 dB and -4.11 dB, the framework with LRI (LSTM) consistently

TABLE XV
LRI PERFORMANCE ON **VGG (LIGHTWEIGHT)** ACROSS **DMRS** DATASETS AT VARIOUS SNRS

VGG(Lightweight) [58], [59]						
SNR	DMRS (Proprietary)					
	ITSP			AT		
	k=2 (I, Q)	LRI(LSTM)	LRI(Trans)	k=2 (I, Q)	LRI(LSTM)	LRI(Trans)
23.37 dB	1.000	1.000	1.000	1.000	1.000	1.000
9.56 dB	1.000	1.000	1.000	1.000	1.000	1.000
-2.51 dB	0.828	**0.941**	0.916	1.348	**1.100**	1.158
-2.74 dB	0.842	**0.930**	0.911	1.322	**1.138**	1.167
-2.81 dB	0.859	**0.937**	0.913	1.284	**1.110**	1.155
-2.99 dB	0.786	**0.907**	0.871	1.471	**1.182**	1.268
-3.13 dB	0.726	**0.881**	0.824	1.635	**1.235**	1.370
-3.42 dB	0.599	**0.834**	0.733	2.076	**1.339**	1.597
-3.7 dB	0.357	0.417	**0.598**	3.005	2.731	**2.019**
-4.11 dB	0.212	0.230	**0.335**	3.818	3.738	**3.161**
AVG	0.721	0.808	**0.810**	1.796	1.557	**1.489**

TABLE XVI
LRI PERFORMANCE ON **INCEPTIONRESNETV2** ACROSS **RADIOML** DATASETS AT VARIOUS SNRS

InceptionResNetV2[61]												
SNR	2016.10A						2018.01A					
	ITSP			AT			ITSP			AT		
	k=2 (I,Q)	LRI(LSTM)	LRI(Trans)	k=2 (I,Q)	LRI(LSTM)	LRI(Trans)	k=2 (I,Q)	LRI(LSTM)	LRI(Trans)	k=2 (I,Q)	LRI(LSTM)	LRI(Trans)
6 dB	0.755	**0.808**	0.699	1.302	**1.206**	1.436	0.889	**0.917**	0.916	1.178	**1.097**	1.101
4 dB	0.785	**0.798**	0.703	1.244	**1.227**	1.405	0.839	0.855	**0.865**	1.239	1.181	**1.172**
2 dB	0.782	**0.799**	0.700	1.256	**1.235**	1.434	0.743	0.746	**0.759**	1.384	1.371	**1.351**
0 dB	0.756	**0.783**	0.672	1.297	**1.261**	1.490	0.614	0.603	**0.616**	**1.789**	1.807	1.795
-2 dB	0.720	**0.734**	0.628	**1.355**	1.366	1.604	0.503	0.502	**0.506**	2.547	**2.479**	2.483
-4 dB	**0.653**	0.634	0.539	**1.553**	1.611	1.976	0.454	**0.456**	0.456	2.991	2.893	**2.872**
-6 dB	0.461	**0.534**	0.445	2.199	**2.024**	2.491	0.381	**0.386**	0.386	3.560	**3.403**	3.361
-8 dB	0.365	**0.405**	0.332	3.050	**2.841**	3.264	**0.291**	0.290	0.289	4.186	**4.030**	4.070
-10 dB	0.248	**0.295**	0.250	3.962	**3.734**	4.078	0.217	**0.231**	0.221	4.777	**4.522**	4.608
-12 dB	0.196	**0.213**	0.186	4.735	**4.478**	4.706	0.150	0.145	**0.152**	5.472	5.278	**5.232**
AVG	0.581	**0.594**	0.592	2.087	**2.031**	2.065	0.524	**0.526**	0.514	**2.834**	2.852	2.894

TABLE XVII
LRI PERFORMANCE ON **INCEPTIONV3** ACROSS **DMRS** DATASETS AT VARIOUS SNRS

IncpetionV3 [60]						
SNR	DMRS (Proprietary)					
	ITSP			AT		
	k=2 (I,Q)	LRI(LSTM)	LRI(Trans)	k=2 (I,Q)	LRI(LSTM)	LRI(Trans)
23.37 dB	1.000	1.000	1.000	1.000	1.000	1.000
9.56 dB	1.000	1.000	1.000	1.000	1.000	1.000
-2.51 dB	0.934	**0.951**	0.943	1.142	**1.104**	1.120
-2.74 dB	0.937	0.937	**0.942**	1.128	1.147	**1.127**
-2.81 dB	0.935	0.942	**0.952**	1.131	1.132	**1.099**
-2.99 dB	0.904	0.920	**0.921**	1.201	1.182	**1.158**
-3.13 dB	0.859	0.876	**0.907**	1.318	1.271	**1.200**
-3.42 dB	0.738	0.803	**0.813**	1.668	1.455	**1.449**
-3.7 dB	0.412	0.481	**0.499**	2.830	2.592	**2.462**
-4.11 dB	0.166	**0.208**	0.189	4.140	**3.903**	3.975
AVG	0.789	0.812	**0.817**	1.656	**1.579**	1.559

TABLE XVIII
LRI PERFORMANCE ON **INCEPTIONRESNETV2** ACROSS **DMRS** DATASETS AT VARIOUS SNRS

IncpetionResNetV2[61]						
SNR	DMRS (Proprietary)					
	ITSP			AT		
	k=2 (I,Q)	LRI(LSTM)	LRI(Trans)	k=2 (I,Q)	LRI(LSTM)	LRI(Trans)
23.37 dB	1.000	1.000	1.000	1.000	1.000	1.000
9.56 dB	1.000	1.000	1.000	1.000	1.000	1.000
-2.51 dB	0.942	0.938	**0.946**	1.094	1.106	**1.093**
-2.74 dB	0.935	0.942	**0.947**	1.110	1.112	**1.097**
-2.81 dB	0.925	0.939	**0.943**	1.131	**1.100**	1.101
-2.99 dB	0.911	0.910	**0.916**	1.158	1.161	**1.156**
-3.13 dB	0.877	0.889	**0.897**	1.232	1.222	**1.197**
-3.42 dB	0.807	0.834	**0.849**	1.411	1.335	**1.311**
-3.7 dB	**0.680**	0.678	0.629	**1.780**	1.800	1.952
-4.11 dB	**0.204**	0.192	0.166	**3.903**	4.027	4.135
AVG	0.828	**0.832**	0.829	**1.482**	1.486	1.504

achieves higher ITSP and efficient Average Trials across all SNR levels. Notably, at SNR levels below -2.99 dB, the ITSP performance with LRI applied demonstrates a sustained improvement of over 0.1 compared to the baseline. Additionally, the Average Trial results indicate enhanced performance over the traditional approach, further underscoring the effectiveness of the LRI method in boosting performance. These findings suggest that the proposed LRI approach exhibits high adaptability to signal variability in real SNR environments.

To validate the performance of LRI in a model capable of extracting more complex and diverse representations than VGG (Lightweight), we utilize InceptionV3. Table XIV illustrates the impact of the proposed LRI technique on the ITSP and AT performance of RadioML under various SNR conditions. In the 2016.10A dataset, the LRI framework demonstrates superior performance, particularly in the Average Trial metric, compared to the baseline. The LRI (LSTM) configuration consistently exceeds baseline performance across most SNR levels, showing a distinct advantage at higher SNRs, such as 6 dB and 4 dB. In terms of ITSP metrics, performance improves with the LRI technique, except at -2 dB and -6 dB. Notably, LRI (LSTM) emerges as the most suitable approach when considering both ITSP and AT. Similar trends are observed in the 2018.01A dataset, where LRI (LSTM) slightly surpasses the baseline in ITSP and AT metrics at high SNR levels, indicating enhanced model efficiency and data transparency in noisy environments. These results suggest that LRI effectively integrates real and imaginary components, enhancing representational capacity in noisy settings. Table XVII compares the ITSP and AT performance of the DMRS dataset with the application of the LRI technique to the InceptionV3 model. Both LRI (Trans) and LRI (LSTM) outperform the baseline configuration in ITSP performance under most SNR conditions, with significant improvements in AT performance, especially at lower SNR levels. The LRI (LSTM) configuration records the lowest average AT value, demonstrating its efficiency and suggesting the potential for LRI techniques in processing complex-valued data in real-world systems.

InceptionV3 demonstrated strong performance across both datasets, but further experimentation with advanced models enhances the reliability of ComplexRep and LRI. Table XVI illustrates the performance of the InceptionResNetV2 model with the application of the LRI technique on the 2016.10A and

2018.01A datasets, specifically regarding ITSP and Average Trial performance. The LRI (LSTM) configuration in the 2016.10A dataset consistently exceeded baseline performance across various SNR levels, notably improving ITSP performance to 0.808 at 6 dB. The Average Trial also showed improvement, recording a minimum value of 1.206 at higher SNRs. Similarly, for the 2018.01A dataset, LRI (LSTM) achieved improvements in ITSP at 0.917 and Average Trial at 1.097 in high SNR conditions. These results indicate that LRI contributes to enhancing the robustness and efficiency of models in complex-valued data processing tasks, suggesting the potential for future applications of the LRI framework in real-world scenarios. Table XVIII presents the performance of the InceptionResNetV2 model when the LRI technique is applied to DMRS. The results show that the LRI (Trans) configuration exhibited excellent performance across various SNR levels, particularly with ITSP scores of 0.946 and 0.947 at -2.51 dB and -2.74 dB, respectively. While there was a slight decrease in the overall average for Average Trial across all SNRs, improvements were observed for most SNR levels, except for a few. These findings suggest the model's capability to deliver reliable results even in complex processing environments. In conclusion, the combination of state-of-the-art models and the LRI technique achieves high performance across diverse SNR conditions while integrating temporal representations, demonstrating its potential for practical applications in real systems.

REFERENCES

[1] Z. Liu, M. Deveci, D. Pamučar, and W. Pedrycz, "An effective multi-source data fusion approach based on α-divergence in belief functions theory with applications to air target recognition and fault diagnosis," *Information Fusion*, vol. 110, p. 102458, 2024.

[2] M. Maimaitijiang, V. Sagan, P. Sidike, S. Hartling, F. Esposito, and F. B. Fritschi, "Soybean yield prediction from uav using multimodal data fusion and deep learning," *Remote sensing of environment*, vol. 237, p. 111599, 2020.

[3] K. Zhang, H. Zhang, and X. Wang, "A hybrid complex spectral conjugate gradient learning algorithm for complex-valued data processing," *Engineering Applications of Artificial Intelligence*, vol. 133, p. 108352, 2024.

[4] Z. Liu, E. Blasch, Z. Xue, J. Zhao, R. Laganiere, and W. Wu, "Objective assessment of multiresolution image fusion algorithms for context enhancement in night vision: a comparative study," *IEEE transactions on pattern analysis and machine intelligence*, vol. 34, no. 1, pp. 94–109, 2011.

[5] H. Zhang, H. Xu, X. Tian, J. Jiang, and J. Ma, "Image fusion meets deep learning: A survey and perspective," *Information Fusion*, vol. 76, pp. 323–336, 2021.

[6] L. Pan, Y. Deng, and D. Pelusi, "A similarity measure of complex-valued evidence theory for multi-source information fusion," *Information Sciences*, vol. 647, p. 119416, 2023.

[7] S. Zhang, Y. Xia, and J. Wang, "A complex-valued projection neural network for constrained optimization of real functions in complex variables," *IEEE Transactions on Neural Networks and Learning Systems*, vol. 26, no. 12, pp. 3227–3238, 2015.

[8] C. Lee, H. Hasegawa, and S. Gao, "Complex-valued neural networks: A comprehensive survey," *IEEE/CAA Journal of Automatica Sinica*, vol. 9, no. 8, pp. 1406–1426, 2022.

[9] A. Kumar, S. Singh, S. Das, and Y. Cao, "Projective quasi-synchronization of complex-valued recurrent neural networks with proportional delay and mismatched parameters via matrix measure approach," *Engineering Applications of Artificial Intelligence*, vol. 126, p. 106800, 2023.

[10] W. Zhao and H. Huang, "Adaptive orthogonal gradient descent algorithm for fully complex-valued neural networks," *Neurocomputing*, vol. 546, p. 126358, 2023.

[11] X. Hou and H. Kayama, *Demodulation reference signal design and channel estimation for LTE-Advanced uplink*. INTECH Open Access Publisher, 2011.

[12] Y.-H. Nam, Y. Akimoto, Y. Kim, M.-i. Lee, K. Bhattad, and A. Ekpenyong, "Evolution of reference signals for lte-advanced systems," *IEEE Communications Magazine*, vol. 50, no. 2, pp. 132–138, 2012.

[13] S.-D. Wang, H.-M. Wang, C. Feng, and V. C. Leung, "Sequential anomaly detection against demodulation reference signal spoofing in 5g nr," *IEEE Transactions on Vehicular Technology*, vol. 72, no. 1, pp. 1291–1295, 2022.

[14] M. M. U. Gul, X. Ma, and S. Lee, "Timing and frequency synchronization for ofdm downlink transmissions using zadoff-chu sequences," *IEEE transactions on Wireless Communications*, vol. 14, no. 3, pp. 1716–1729, 2014.

[15] M. Hua, M. Wang, K. W. Yang, and K. J. Zou, "Analysis of the frequency offset effect on zadoff–chu sequence timing performance," *IEEE Transactions on Communications*, vol. 62, no. 11, pp. 4024–4039, 2014.

[16] F. Wang, T. Shang, C. Hu, and Q. Liu, "Automatic modulation classification using hybrid data augmentation and lightweight neural network," *Sensors*, vol. 23, no. 9, p. 4187, 2023.

[17] R.-A. Pitaval, B. M. Popović, P. Wang, and F. Berggren, "Overcoming 5g prach capacity shortfall: Supersets of zadoff–chu sequences with low-correlation zone," *IEEE Transactions on Communications*, vol. 68, no. 9, pp. 5673–5688, 2020.

[18] J. Kim and O. Jo, "Incepseqnet: Advancing signal classification with multi-shape augmentation (student abstract)," in *Proceedings of the AAAI Conference on Artificial Intelligence*, vol. 38, pp. 23542–23543, 2024.

[19] X. Xie, C. Li, T. Guan, Y. Zheng, and X. Wu, "A novel complex-valued convolutional network for real-world single image dehazing," *Journal of Visual Communication and Image Representation*, vol. 97, p. 103984, 2023.

[20] J. Joung and B. C. Jung, "Machine learning based blind decoding for space–time line code (stlc) systems," *IEEE Transactions on Vehicular Technology*, vol. 68, no. 5, pp. 5154–5158, 2019.

[21] L. Shen, Y.-D. Yao, H. Wang, and H. Wang, "Blind decoding based on independent component analysis for a massive mimo uplink system in microcell rician/rayleigh fading channels," *IEEE Transactions on Vehicular Technology*, vol. 65, no. 10, pp. 8322–8330, 2015.

[22] X. Zha, H. Peng, X. Qin, G. Li, and S. Yang, "A deep learning framework for signal detection and modulation classification," *Sensors*, vol. 19, no. 18, p. 4042, 2019.

[23] W. Zhang, M. Feng, M. Krunz, and A. H. Y. Abyaneh, "Signal detection and classification in shared spectrum: A deep learning approach," in *IEEE INFOCOM 2021-IEEE Conference on Computer Communications*, pp. 1–10, IEEE, 2021.

[24] Z. Chen, H. Cui, J. Xiang, K. Qiu, L. Huang, S. Zheng, S. Chen, Q. Xuan, and X. Yang, "Signet: A novel deep learning framework for radio signal classification," *IEEE Transactions on Cognitive Communications and Networking*, vol. 8, no. 2, pp. 529–541, 2021.

[25] U. Mutlu and Y. Kabalci, "Deep learning aided channel estimation approach for 5g communication systems," in *2022 4th Global Power, Energy and Communication Conference (GPECOM)*, pp. 655–660, IEEE, 2022.

[26] Y. Wang, G. Gui, H. Gacanin, T. Ohtsuki, O. A. Dobre, and H. V. Poor, "An efficient specific emitter identification method based on complex-valued neural networks and network compression," *IEEE Journal on Selected Areas in Communications*, vol. 39, no. 8, pp. 2305–2317, 2021.

[27] S. Kang, T. Lee, J. Kim, J. Kim, O. Jo, *et al.*, "Intelligent index classification method based on machine learning for detection of reference signal in 5g networks," *IEEE Access*, 2023.

[28] T. Ya, L. Yun, Z. Haoran, J. Zhang, W. Yu, G. Guan, and M. Shiwen, "Large-scale real-world radio signal recognition with deep learning," *Chinese Journal of Aeronautics*, vol. 35, no. 9, pp. 35–48, 2022.

[29] S. Ji and M. Li, "Clnet: Complex input lightweight neural network designed for massive mimo csi feedback," *IEEE Wireless Communications Letters*, vol. 10, no. 10, pp. 2318–2322, 2021.

[30] T. Erpek, T. J. O'Shea, Y. E. Sagduyu, Y. Shi, and T. C. Clancy, "Deep learning for wireless communications," *Development and Analysis of Deep Learning Architectures*, pp. 223–266, 2020.

[31] S. W. Kang and O. Jo, "Multivariate time-series imagification with time embedding in constrained environments (student abstract)," in *Proceedings of the AAAI Conference on Artificial Intelligence*, vol. 38, pp. 23535–23536, 2024.

[32] Z. Zhao, M. C. Vuran, F. Guo, and S. D. Scott, "Deep-waveform: A learned ofdm receiver based on deep complex-valued convolutional

networks," *IEEE Journal on Selected Areas in Communications*, vol. 39, no. 8, pp. 2407–2420, 2021.
[33] S. Peng, S. Sun, and Y.-D. Yao, "A survey of modulation classification using deep learning: Signal representation and data preprocessing," *IEEE Transactions on Neural Networks and Learning Systems*, vol. 33, no. 12, pp. 7020–7038, 2021.
[34] S. Hanna, C. Dick, and D. Cabric, "Signal processing-based deep learning for blind symbol decoding and modulation classification," *IEEE Journal on Selected Areas in Communications*, vol. 40, no. 1, pp. 82–96, 2021.
[35] S. Zheng, S. Chen, P. Qi, H. Zhou, and X. Yang, "Spectrum sensing based on deep learning classification for cognitive radios," *China Communications*, vol. 17, no. 2, pp. 138–148, 2020.
[36] Y. Tian, C. Li, and S. Yang, "Deep learning model for demodulation reference signal based channel estimation," *arXiv preprint arXiv:2109.10667*, 2021.
[37] J. Zhang, F. Wu, B. Wei, Q. Zhang, H. Huang, S. W. Shah, and J. Cheng, "Data augmentation and dense-lstm for human activity recognition using wifi signal," *IEEE Internet of Things Journal*, vol. 8, no. 6, pp. 4628–4641, 2020.
[38] M. Patel, X. Wang, and S. Mao, "Data augmentation with conditional gan for automatic modulation classification," in *Proceedings of the 2nd ACM Workshop on wireless security and machine learning*, pp. 31–36, 2020.
[39] C. Yu, R. Han, M. Song, C. Liu, and C.-I. Chang, "A simplified 2d-3d cnn architecture for hyperspectral image classification based on spatial–spectral fusion," *IEEE Journal of Selected Topics in Applied Earth Observations and Remote Sensing*, vol. 13, pp. 2485–2501, 2020.
[40] M. Hussain, J. J. Bird, and D. R. Faria, "A study on cnn transfer learning for image classification," in *Advances in Computational Intelligence Systems: Contributions Presented at the 18th UK Workshop on Computational Intelligence, September 5-7, 2018, Nottingham, UK*, pp. 191–202, Springer, 2019.
[41] S. Zheng, P. Qi, S. Chen, and X. Yang, "Fusion methods for cnn-based automatic modulation classification," *IEEE Access*, vol. 7, pp. 66496–66504, 2019.
[42] P. Dong, H. Zhang, G. Y. Li, I. S. Gaspar, and N. NaderiAlizadeh, "Deep cnn-based channel estimation for mmwave massive mimo systems," *IEEE Journal of Selected Topics in Signal Processing*, vol. 13, no. 5, pp. 989–1000, 2019.
[43] D. Zhang, Y. Lu, Y. Li, W. Ding, and B. Zhang, "High-order convolutional attention networks for automatic modulation classification in communication," *IEEE Transactions on Wireless Communications*, 2022.
[44] J. Nie, Y. Zhang, Z. He, S. Chen, S. Gong, and W. Zhang, "Deep hierarchical network for automatic modulation classification," *IEEE Access*, vol. 7, pp. 94604–94613, 2019.
[45] A. P. Hermawan, R. R. Ginanjar, D.-S. Kim, and J.-M. Lee, "Cnn-based automatic modulation classification for beyond 5g communications," *IEEE Communications Letters*, vol. 24, no. 5, pp. 1038–1041, 2020.
[46] J. Y. Han, O. Jo, and J. Kim, "Exploitation of channel-learning for enhancing 5g blind beam index detection," *IEEE Transactions on Vehicular Technology*, vol. 71, no. 3, pp. 2925–2938, 2022.
[47] T. J. O'Shea, T. Roy, and T. C. Clancy, "Over-the-air deep learning based radio signal classification," *IEEE Journal of Selected Topics in Signal Processing*, vol. 12, no. 1, pp. 168–179, 2018.
[48] V.-H. Nguyen, M.-T. Nguyen, J. Choi, and Y.-H. Kim, "Nlos identification in wlans using deep lstm with cnn features," *Sensors*, vol. 18, no. 11, p. 4057, 2018.
[49] J. Xie, J. Fang, C. Liu, and X. Li, "Deep learning-based spectrum sensing in cognitive radio: A cnn-lstm approach," *IEEE Communications Letters*, vol. 24, no. 10, pp. 2196–2200, 2020.
[50] J. Ma, Y. Jing, Z. Yang, H. Yang, and Z. Wu, "Shuffleformer: An efficient shuffle meta framework for automatic modulation classification," *Physical Communication*, vol. 61, p. 102226, 2023.
[51] Q. Zheng, P. Zhao, H. Wang, A. Elhanashi, and S. Saponara, "Fine-grained modulation classification using multi-scale radio transformer with dual-channel representation," *IEEE Communications Letters*, vol. 26, no. 6, pp. 1298–1302, 2022.
[52] J. Cai, F. Gan, X. Cao, and W. Liu, "Signal modulation classification based on the transformer network," *IEEE Transactions on Cognitive Communications and Networking*, vol. 8, no. 3, pp. 1348–1357, 2022.
[53] Q. Zhou, X. Jing, Y. He, Y. Cui, M. Kadoch, and M. Cheriet, "Lstm-based automatic modulation classification," in *2020 IEEE International Symposium on Broadband Multimedia Systems and Broadcasting (BMSB)*, pp. 1–4, IEEE, 2020.
[54] A. Vaswani, "Attention is all you need," *Advances in Neural Information Processing Systems*, 2017.
[55] T. J. O'Shea, T. Roy, and T. C. Clancy, "Over-the-air deep learning based radio signal classification," *IEEE Journal of Selected Topics in Signal Processing*, vol. 12, no. 1, pp. 168–179, 2018.
[56] Q. Zheng, X. Tian, Z. Yu, H. Wang, A. Elhanashi, and S. Saponara, "Dl-pr: Generalized automatic modulation classification method based on deep learning with priori regularization," *Engineering Applications of Artificial Intelligence*, vol. 122, p. 106082, 2023.
[57] M. Grandini, E. Bagli, and G. Visani, "Metrics for multi-class classification: an overview," *arXiv preprint arXiv:2008.05756*, 2020.
[58] J. Kim and O. Jo, "Mushaug: Boosting sequence signal classification via multishape augmentation," *IEEE Internet of Things Journal*, vol. 11, no. 20, pp. 32585–32597, 2024.
[59] K. Simonyan and A. Zisserman, "Very deep convolutional networks for large-scale image recognition," *arXiv preprint arXiv:1409.1556*, 2014.
[60] C. Szegedy, V. Vanhoucke, S. Ioffe, J. Shlens, and Z. Wojna, "Rethinking the inception architecture for computer vision," in *Proceedings of the IEEE conference on computer vision and pattern recognition*, pp. 2818–2826, 2016.
[61] C. Szegedy, S. Ioffe, V. Vanhoucke, and A. Alemi, "Inception-v4, inception-resnet and the impact of residual connections on learning," in *Proceedings of the AAAI conference on artificial intelligence*, vol. 31, 2017.

Jongseok Kim Jongseok Kim (Student Member, IEEE) received his bachelor's degree in science engineering from Chungbuk National University in South Korea in 2023. He is currently pursing a master's degree in computer science. During his undergraduate years, he worked as a research assistant at Professor Ohyun Jo's Information System Laboratory. His research interests include signal recognition and estimation, signal generation for denosing, data augmentation optimization, and lightweight model optimization.

Woonggyu Min Woongyu Min (Student Member, IEEE) recieved the B.S. degree in the Department of Computer Science at Chungbuk National University, Chungju, South Korea, in 2024, respectively, where he is currently pursuing the M.S. degree with the Department of Computer Science. Currently, he works at Information System Lab, Chungbuk national university. His current research interests are deep learning, Larger Language Model, Data Denoising.

Juyeop Kim Juyeop Kim (Member, IEEE) received the B.S. and Ph.D. degrees in electrical engineering from the Korea Advanced Institute of Science and Technology (KAIST), Daejeon, South Korea, in 2004 and 2010, respectively. He is currently an Assistant Professor with the Department of Electronics Engineering, Sookmyung Women's University, Seoul, South Korea. From 2010 to 2011, he was with KAIST Institute IT Convergence Research Center in charge of research for 5G cellular system. From 2011 to 2013, he was with Samsung Electronics in charge of development and commercialization for 2G/3G/4G multimode mobile modem solution. From 2014 to 2018, he was with the Korea Railroad Research Institute in charge of research and development for LTE-Railway(LTE-R), Public Safety LTE (PS-LTE) and railway IoT solutions. His current research interests include the applied wireless communications including mission critical communications, Internet of Things, and software-defined modems.

Ohyun Jo Ohyun Jo (Member, IEEE) received the B.S., M.S., and Ph.D. degrees in electrical engineering from the Korea Advanced Institute of Science and Technology, Daejeon, South Korea, in 2005, 2007, and 2011, respectively. He is currently an Associate Professor with the Department of Computer Science, Chungbuk National University, Cheongju, South Korea. From April 2011 to February 2016, he was with the Samsung Electronics in charge of research and development for future wireless communication systems, applications, and services. From March 2016 to July 2017, he was a Senior Researcher with Electronics and Telecommunications Research Institute and from August 2017 to February 2018, he was an Assistant Professor with the Department of Electrical Engineering, Korea Military Academy. He has authored and coauthored more than 90 papers, and holds more than 170 registered and filed patents. During his appointment with Samsung, he was the recipient of numerous recognitions, including the Gold Prize in Samsung Annual Award, Most Creative Researcher of the Year Award, Best Mentoring Award, Major R&D Achievement Award, and Best Improvement of Organization Culture Award. His research interests include machine learning applications, next generation mobile communication systems, military communications, Internet of Things, future wireless solutions/applications/services, and embedded communications ASIC design.